Rapid Communications

Multiple spin-orbit excitons and the electronic structure of α-$RuCl_3$

P. Warzanowski,[1] N. Borgwardt,[1] K. Hopfer,[1] J. Attig,[2] T. C. Koethe,[1] P. Becker,[3] V. Tsurkan,[4,5] A. Loidl,[4] M. Hermanns,[6,7] P. H. M. van Loosdrecht,[1] and M. Grüninger[1]

[1]*Institute of Physics II, University of Cologne, D-50937 Cologne, Germany*
[2]*Institute for Theoretical Physics, University of Cologne, D-50937 Cologne, Germany*
[3]*Section Crystallography, Institute of Geology and Mineralogy, University of Cologne, D-50674 Cologne, Germany*
[4]*Experimental Physics V, Center for Electronic Correlations and Magnetism, University of Augsburg, D-86135 Augsburg, Germany*
[5]*Institute of Applied Physics, MD-2028 Chisinau, Moldova*
[6]*Department of Physics, Stockholm University, AlbaNova University Center, SE-106 91 Stockholm, Sweden*
[7]*Nordita, KTH Royal Institute of Technology and Stockholm University, SE-106 91 Stockholm, Sweden*

(Received 20 November 2019; accepted 21 September 2020; published 13 October 2020)

The honeycomb compound α-$RuCl_3$ is widely discussed as a proximate Kitaev spin-liquid material. This scenario builds on spin-orbit entangled $j = 1/2$ moments arising for a t_{2g}^5 electron configuration with strong spin-orbit coupling λ and a large cubic crystal field. The actual low-energy electronic structure of α-$RuCl_3$, however, is still puzzling. In particular, infrared absorption features at 0.30, 0.53, and 0.75 eV seem to be at odds with a $j = 1/2$ scenario. Also the energy of the spin-orbit exciton, the excitation from $j = 1/2$ to $3/2$, and thus the value of λ, are controversial. Combining infrared and Raman data, we show that the infrared features can be attributed to single, double, and triple spin-orbit excitons. We find $\lambda = 0.16$ eV and $\Delta = 42(4)$ meV for the observed noncubic crystal-field splitting, supporting the validity of the $j = 1/2$ picture for α-$RuCl_3$. The unusual strength of the double excitation is related to the underlying hopping interactions, which form the basis for dominant Kitaev exchange.

DOI: 10.1103/PhysRevResearch.2.042007

The exactly solvable Kitaev model [1] describes bond-anisotropic exchange interactions on tricoordinated lattices. Exchange frustration embodied in the model yields a rich phase diagram with gapless and gapped quantum spin liquids in which spins fractionalize into emergent Majorana fermions and gauge fluxes. Gapless Majorana fermions form a metal which on a honeycomb lattice is equivalent to magnetic Dirac matter [2]. Jackeli and Khaliullin [3] demonstrated that the Kitaev model may be realized in honeycomb compounds such as Na_2IrO_3 or α-$RuCl_3$ [4] with edge-sharing IrO_6 or $RuCl_6$ octahedra, t_{2g}^5 configuration, and strong spin-orbit coupling. This triggered an avalanche of experimental and theoretical research [5–10].

At low temperatures, α-$RuCl_3$ orders magnetically due to exchange interactions beyond the Kitaev model [11–13]. The term proximate Kitaev spin liquid [14] was coined for α-$RuCl_3$ based on fingerprints of dominant Kitaev interactions in spectroscopy, e.g., above the magnetic ordering temperature. In particular, inelastic neutron scattering, Raman scattering, and THz spectroscopy revealed an intriguing continuum of magnetic excitations [14–21] for which a fermionic character [18,21] and the restriction of dynamical spin-spin correlations to nearest neighbors [15] were reported. However, a more conventional interpretation in terms of overdamped magnons has also been proposed [13]. The Kitaev picture is in line with the stunning claim of a half-quantized thermal Hall effect [22].

In the light of these far-reaching results, it is surprising that the low-energy electronic structure of α-$RuCl_3$ remains controversial. In the related iridates, the approximate validity of the $j = 1/2$ scenario is well established by resonant inelastic x-ray scattering (RIXS) data of the spin-orbit exciton [23–27], i.e., the excitation to $j = 3/2$, but high-resolution RIXS at the Ru L or M edges is challenging [28,29]. In α-$RuCl_3$, conflicting energies of 145, 195, and 231 meV were reported for the spin-orbit exciton by Raman, inelastic neutron scattering, and Ru M edge RIXS, respectively [14,29,30]. Furthermore, several groups reported on infrared absorption bands at 0.30, 0.53, and 0.75 eV [4,30–35]. The 0.30 eV peak was assigned to the Mott gap [4,33,34], but a gap of about 1 eV is well established by different techniques [30–32,36–41]. Thus far, there is no convincing explanation for this multitude of excitations below the gap.

A scenario first proposed in 1971 attributes the infrared features to $t_{2g}^4 e_g^1$ excited states [30–32,34,41]. This contradicts results of quantum chemistry and spectroscopy [39,42,43] which show the $t_{2g}^4 e_g^1$ states above 1.3 eV. Low-lying e_g states would severely affect exchange interactions and the role of Kitaev coupling [3,44]. Alternatively, the infrared bands were discussed as possible evidence for a large non-cubic crystal-field splitting $\Delta \approx 180$ meV [35], which contrasts with the much smaller values found by x-ray absorption, $\Delta \approx -10$ meV [42], quantum chemistry,

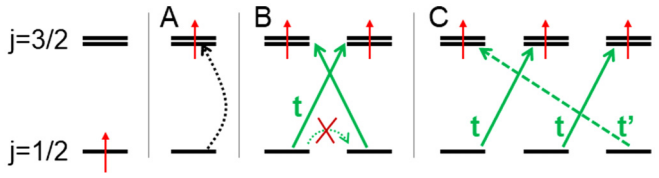

FIG. 1. Sketch of the different excitations from a ground state with $j = 1/2$ moments on each site. The spin-orbit exciton, peak A in Fig. 2, is an on-site excitation from $j = 1/2$ to 3/2. A double spin-orbit exciton, peak B, results from the exchange of two holes between adjacent sites. Nearest-neighbor hopping t (solid green arrows) connects $j = 1/2$ and 3/2 on adjacent sites, it is suppressed between $j = 1/2$ states. The triple process, peak C, involves hopping t' between next-nearest neighbors. The sketch neglects the noncubic crystal field.

$\Delta = 39$ meV [43], density functional theory, $\Delta = 37$ meV [45,46], and M edge RIXS, $\Delta < 40$ meV [29]. Note that $\Delta \approx 180$ meV would strongly mix $j = 1/2$ and 3/2 states, again with dramatic consequences for the exchange interactions [7,47]. Finally, an exact diagonalization study interpreted the 0.3 eV peak as the spin-orbit exciton, activated by direct d-d intersite hopping [48], leaving the features at 0.53 and 0.75 eV unexplained.

In this Rapid Communication, we report on infrared absorption and Raman scattering measurements which resolve the puzzle. Our Raman data feature the spin-orbit exciton, split by the non-cubic crystal field, at 248 and 290 meV. The three infrared bands correspond to phonon-assisted excitations of single and double spin-orbit excitons and the direct excitation of a triple spin-orbit exciton (see Fig. 1). We find that the phonon-assisted excitation of double spin-orbit excitons in Kitaev materials is closely related to the Lorenzana-Sawatzky-type two-magnon-plus-phonon absorption in the high-T_c cuprate parent compounds [49,50]. Our data yield $\lambda = 0.16$ eV within the Ru $4d$ shell. The ratio of noncubic crystal-field splitting and λ is very similar to the case of Na_2IrO_3, supporting the validity of the $j = 1/2$ picture in α-$RuCl_3$.

Single crystals of α-$RuCl_3$ were prepared by sublimation growth in evacuated SiO_2 glass ampoules after purification of the compound by recrystallization in vacuum. Infrared transmittance was measured using a Bruker IFS 66/v Fourier-transform spectrometer equipped with a ^{4}He cryostat. We studied samples with a thickness of (67 ± 5) and (30 ± 3) μm. The polarization of the electric field was parallel to the honeycomb layers. We used the Fabry-Perot interference fringes to determine the refractive index n, which is approximately constant for frequencies below the Mott gap and far above the phonons. Knowing $n(\omega)$ and transmittance $T(\omega)$, one can calculate the optical conductivity $\sigma_1(\omega)$. Raman measurements were performed in backscattering geometry using a micro-Raman setup with a TriVista spectrometer and an incident laser wavelength of 462 nm.

We compare the optical conductivity $\sigma_1(\omega)$ and the Raman data in Fig. 2. In α-$RuCl_3$, phonons are restricted to below 40 meV [16,34,35] and the energy of magnetic excitations is even smaller [14–16]. Above 0.9 eV, $\sigma_1(\omega)$ shows the onset of excitations across the Mott gap, reaching about 10^3 $(\Omega\,\mathrm{cm})^{-1}$

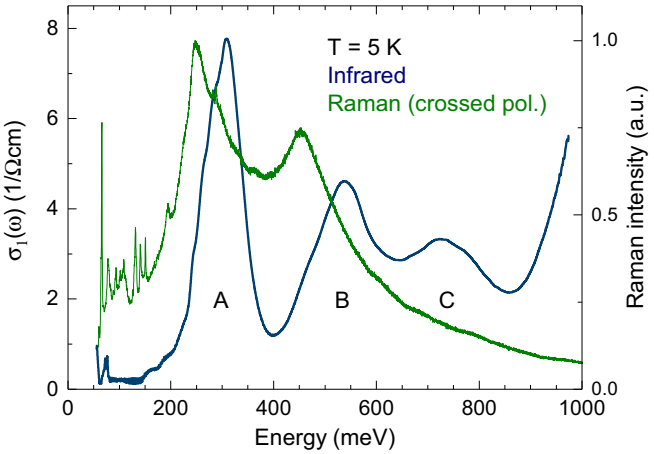

FIG. 2. Optical conductivity $\sigma_1(\omega)$ (left axis) and Raman data (right) of α-$RuCl_3$. Features A, B, and C correspond to (phonon-assisted) single, double, and triple spin-orbit excitons, respectively, cf. Fig. 1. The increase of $\sigma_1(\omega)$ above 0.9 eV indicates the Mott gap. Above 1 eV, $\sigma_1(\omega)$ reaches about 10^3 $(\Omega\,\mathrm{cm})^{-1}$ [38,41]. The much smaller values of $\sigma_1(\omega)$ below the gap are typical for weak phonon-assisted or higher-order absorption features [53].

above 1 eV [30–32,36–41]. The prominent infrared peaks A, B, and C at 0.30, 0.53, and 0.75 eV agree very well with previous reports [4,30–35], demonstrating that these features reflect the local electronic structure. They are robust against the widely discussed sample issues in α-$RuCl_3$ which are related to the stacking sequence of honeycomb layers [35]. Our Raman data reveal two strong peaks at 248 meV and 450 meV and a clear shoulder at 290 meV. The pronounced difference between infrared and Raman spectra originates from the selection rules, offering a key to the assignment.

A given mode is Raman active if it modulates the polarizability and infrared active if it carries an electric dipole moment. The spin-orbit exciton is a local excitation between $4d$ orbitals (see Fig. 1). It is closely related to an on-site d-d excitation. Its Raman activity was demonstrated in Sr_2IrO_4 [51]. Such an electronic transition between even d orbitals does not carry a dipole moment but becomes infrared active by the simultaneous excitation of a symmetry-breaking phonon [52,53]. Such phonon-assisted infrared excitations from $j = 1/2$ to 3/2 were observed in host crystals doped with $5d^5$ Ir^{4+} ions [54], equivalent to $4d^5$ Ru^{3+}. In the honeycomb lattice the Ru sites do not show inversion symmetry. However, the corresponding admixture of p or odd character to the d orbitals usually is neglected. We thus expect the infrared peak of the spin-orbit exciton to be shifted with respect to the Raman peak by a phonon frequency, as observed for peak A.

For phonon-assisted features located between ω_1 and ω_2, the phonon energy $\hbar\omega_{\mathrm{ph}}$ can be determined by the temperature dependence of the spectral weight (SW) [52],

$$SW = \int_{\omega_1}^{\omega_2} \sigma_1(\omega)\, d\omega = \alpha + \beta \coth\left(\frac{\hbar\omega_{\mathrm{ph}}}{2k_B T}\right), \qquad (1)$$

where α and β are fit parameters. Thermal population of the phonon yields an increase of SW. Figure 3 depicts the temperature dependence of $\sigma_1(\omega)$. Figure 4(a) shows SW of peaks A, B, and C. The spectral weight of peak C is constant below

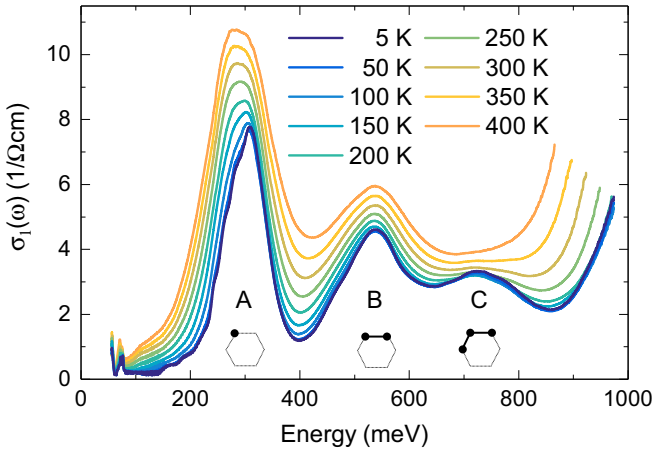

FIG. 3. Temperature dependence of $\sigma_1(\omega)$. With increasing temperature, the Mott gap softens or smears out, partially covering peak C, while peaks A and B show a pronounced increase of spectral weight, typical for phonon-assisted excitations [see Fig. 4(a)]. The high-energy cutoff reflects the suppression of the measured transmittance. Sketches denote the different excitations (cf. Fig. 1).

200 K. The increase above 200 K is due to the softening of the gap, see Fig. 3. Accordingly, peak C is not phonon-assisted but directly infrared active, in agreement with the absence of a corresponding Raman feature. For peaks A and B, fits using Eq. (1) yield $\hbar\omega_{\rm ph} = 19.6$ meV and 39.3 meV, respectively [see Fig. 4(a)] [55]. Note that excitations across the gap have a negligible effect on SW of peaks A and B. An independent analysis of the temperature dependence of $\sigma_1(\omega)$ using an oscillator model (not shown) yields very similar results for the frequencies of the symmetry-breaking phonons.

The phonon energies of 19.6 and 39.3 meV agree with phonon studies using Raman and infrared spectroscopy

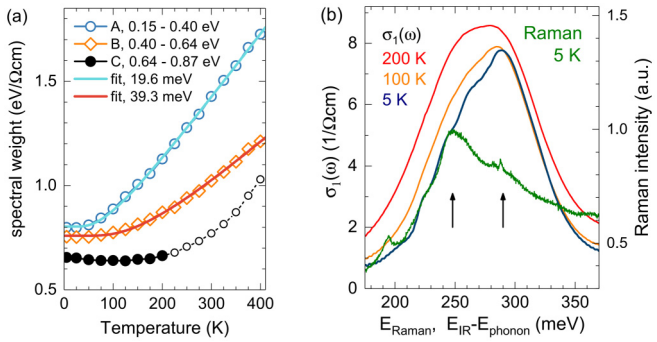

FIG. 4. Spectral weight (left) and zoom in on peak A (right). (a) Using Eq. (1), fits of the spectral weight, integrated over the indicated ranges, yield $\hbar\omega_{\rm ph} = 19.6$ meV for peak A and 39.3 meV for peak B. For peak C, the behavior above 200 K (small symbols) is hidden by the softening of the gap (cf. Fig. 3) while the spectral weight below 200 K (solid symbols) is independent of temperature. (b) Green: Raman data (right axis). Other curves: $\sigma_1(\omega)$ (left axis), shifted by 20 meV to compensate for the phonon shift $\hbar\omega_{\rm ph}$ of the phonon-assisted process. Arrows at 248 and 290 meV indicate peak positions of the spin-orbit exciton split by the noncubic crystal field. Additional phonon sidebands reflect the vibronic character.

[16,34,35]. The fact that two phonon energies are observed is remarkable. It is hard to reconcile with the scenario of excitations to various $t_{2g}^4\, e_g^1$ multiplets [30–32,34,41], because the phonon should be equally effective in breaking the symmetry for all on-site excitations. However, two different phonon modes have to be expected if we assign peaks A and B to single and double spin-orbit excitons. The former is an on-site process for which a phonon has to break the symmetry (on the honeycomb lattice: enhance the odd-symmetry character) on a Ru site. The double excitation, in contrast, involves the exchange of holes between two neighboring sites and becomes infrared active via a different phonon mode breaking the symmetry between a Ru-Ru pair. Note that this scenario of (multiple) spin-orbit excitons — excitations within the t_{2g} shell — is the only plausible explanation for the observed features, considering the accepted energy scales (see above) of phonons, magnons, the Mott gap, and the t_{2g}-e_g splitting.

Single spin-orbit exciton. The closer look on peak A provided in Fig. 4(b) strongly supports its spin-orbit exciton nature. As discussed in the following, its energy yields a reasonable value of λ, and the data support the phonon shift between Raman and infrared data as well as the vibronic character expected for an excitation involving orbitals. Shifting the infrared data by 20 meV to compensate for the phonon-assisted character, we find a stunning agreement with the Raman data which peak at 248 meV and show a second feature at 290 meV. Both coincide with peaks in the shifted infrared data. The data show further sidebands shifted by 19 meV. These can be understood as vibronic sidebands according to the Franck-Condon principle [52,53]. The $j = 1/2$ ground state and the $j = 3/2$ excited state differ in the spatial distributions of electronic charge and thus also in the relaxed configurations of the lattice [56]. Therefore, these excitations mix with phonons, which causes phonon sidebands. We emphasize that this vibronic mixture is a property of the eigenstates which is independent of the spectroscopic technique. In particular, the phonon sidebands should not be confused with the additional phonon that is necessary for breaking the symmetry in the infrared case.

The spin-orbit exciton can be described by the single-site Hamiltonian for the t_{2g} states [3,57],

$$H_{\rm single} = \lambda_{\rm eff}\, \mathbf{S}\cdot\mathbf{L} + \Delta_{\rm CF}\, L^2_{[111]}\,, \qquad (2)$$

where $L_{[111]}$ denotes the component of $\mathbf{L}$ along the trigonal [111] axis. The trigonal crystal field parameterized by $\Delta_{\rm CF}$ yields a splitting of the excited $j = 3/2$ quartet. For $\Delta_{\rm CF}/\lambda_{\rm eff} \ll 1$, the observed splitting is $\Delta = \frac{2}{3}\Delta_{\rm CF}$. With Raman peaks at 248(1) meV and 290(4) meV, there are two different solutions of Eq. (2), $\lambda_{\rm eff} = 175(1)$ meV and $\Delta_{\rm CF} = 70(9)$ meV for trigonal elongation, or $\lambda_{\rm eff} = 177(1)$ meV and $\Delta_{\rm CF} = -59(7)$ meV for compression. Accordingly, the $j = 1/2$ wave function carries more than 98 % of the weight of the local ground state, corroborating the applicability of the $j = 1/2$ picture for α-$RuCl_3$. The ratio $\Delta/\lambda_{\rm eff} \approx 1/4.5$ is very similar in Na_2IrO_3, where RIXS finds $\lambda_{\rm eff} = 0.4$–0.5 eV and $\Delta = 0.11$ eV [25].

Quantum chemistry calculations predicted the spin-orbit exciton at 195 meV and 234 meV with a splitting $\Delta =$ 39 meV [43]. These values, in particular the splitting, agree

very well with our result. Density functional theory finds $\Delta = 37$ meV [45,46], while a somewhat smaller splitting of $\Delta_{\mathrm{CF}} = (-12 \pm 10)$ meV was derived from linear dichroism in x-ray absorption spectroscopy [42]. Note that our experimental splitting $\Delta = 42(4)$ meV is still smaller than the vibronic peak width, and one may speculate whether the considerable overlap of the two excitations explains the reduced dichroism. With the currently available resolution, RIXS data measured at the Ru M edge at 300 K support our assignment of peak A but cannot resolve the splitting [29].

The effective parameter $\lambda_{\mathrm{eff}} \approx 176$ meV applies to the single-site Hamiltonian restricted to t_{2g} orbitals, Eq. (2). Considering the full $4d$ shell including the e_g orbitals with $10\,\mathrm{Dq} = 2.2$ eV [30,39], we find $\lambda = 0.16$ eV. In the literature on α-$RuCl_3$, typical values for λ fall in the range 0.13–0.15 eV [29,37,42,44,58], but a precise experimental value was missing thus far.

Our interpretation of peak A as spin-orbit exciton poses the question of the origin of the features at lower energy that previously were attributed to this excitation. The claim of a neutron mode at 195 meV [14] needs to be substantiated by high-energy neutron data with improved signal-to-noise ratio. In Raman scattering with a 532-nm laser, a weak mode was reported at 145 meV [30]. Our Raman data show a multitude of weak modes below 200 meV, see Fig. 2. In particular we find three narrow peaks at 131, 141, and 151 meV. We tentatively attribute all of these weak features to multiphonon excitations. Their strength depends on the laser wavelength and the sample quality and may be boosted by a flat phonon dispersion. In the infrared data, the feature at 73 meV, i.e., about half the energy, has been explained as a strong two-phonon excitation [34].

Double spin-orbit exciton. To explain this process, we consider the phonon-assisted two-magnon absorption described by Lorenzana and Sawatzky [49,50]. It is a powerful tool for the study of magnetic excitations in, e.g., the $S = 1/2$ cuprate parent compounds [59]. There, exchanging two antiparallel spins on adjacent sites is equivalent to a double spin flip. This process is Raman active but does not carry a dipole moment. It becomes infrared active by the simultaneous excitation of a high-energy breathing phonon which yields different on-site energies on the two sites, breaking the symmetry on the bond. In the edge-sharing geometry of α-$RuCl_3$, this role is played by the highest E_u phonon mode [34], which agrees with our result $\hbar\omega_{\mathrm{ph}} = 39$ meV for peak B. The spectral weight in $\sigma_1(\omega)$ is proportional to the effective charge $q_{\mathrm{eff}} = \frac{\partial^2 J}{\partial u\, \partial |\mathbf{E}|}$ where J denotes the exchange coupling constant, u the ionic displacement, and $\mathbf{E}$ the applied electric field. For α-$RuCl_3$, we estimate the order of magnitude of the leading-order contribution [60], which yields similar results as in the cuprates. Experimentally, peak B reaches about 4 $(\Omega\,\mathrm{cm})^{-1}$ and has a width of about 0.1 eV. Indeed, similar spectral weights are found in the cuprates [59].

Compared to magnetic excitations, the observation of a double excitation involving orbitals is unusual but not unprecedented. The strength of this process depends on the particular form of intersite hopping. For the two-magnon process in the cuprates, it is sufficient to consider a half-filled x^2-y^2 orbital per site and hopping between them. In contrast, the double-orbital excitation is boosted if hopping predominantly connects the ground state orbital on site i with an excited orbital on site j. For instance, two-orbiton infrared absorption was observed in the Mott insulator YVO_3 [61] which shows antiferro-orbital order of xz and yz along c. Hopping between adjacent sites i and j is diagonal in xz and yz. Starting from $|0\rangle = |xz\rangle_i\,|yz\rangle_j$, the exchange of electrons leads to the final state $|yz\rangle_i\,|xz\rangle_j$ with orbital excitations on both sites. In α-$RuCl_3$, the double excitation proceeds via a similar path. Nearest-neighbor hopping from $|j = 1/2\rangle_i$ is only finite to $|3/2\rangle_j$ but vanishes to $|1/2\rangle_j$ (see Fig. 1). From $|0\rangle = |1/2\rangle_i\,|1/2\rangle_j$, the leading contribution of particle exchange yields $|3/2\rangle_i|3/2\rangle_j$, the double spin-orbit exciton. Interaction effects change this picture only slightly, the double spin-orbit exciton remains the dominant contribution (see Supplemental Material [62]). This property of the hopping interactions is the source for vanishing Heisenberg and dominant Kitaev exchange [3]. In this sense, the strength of the double excitation is a direct consequence of dominant Kitaev exchange.

The precise energy of the double excitation is more subtle. Naively, one may expect combination tones of 248 and 290 meV. However, for the double excitation one has to consider dispersion, even if the total wavevector has to vanish, and in particular interaction effects. For two-magnon absorption, this dramatically affects the peak energies, in particular in the case of bound states [63]. In α-$RuCl_3$, it is, e.g., feasible to consider a lattice distortion which lowers the spin-orbit exciton excitation energy on both sites. The observed energies of 450 meV in Raman scattering and $(490 + 39)$ meV in infrared absorption are thus plausible. Following Fig. 1, the infrared peak invokes excitations to $|3/2\rangle_i|3/2\rangle_j$ due to nearest-neighbor hopping t. Raman scattering proceeds via a high-energy intermediate state which may favor a different flavor of the double spin-orbit exciton, explaining the lower energy. A thorough investigation of interaction effects is beyond the scope of our study, which is focused on the detection and identification of the double spin-orbit exciton. Note, however, that our assignment is supported by exact diagonalization of a two-site cluster which reproduces the observed Raman energies (see Supplemental Material [62]). In the related iridates, RIXS at the Ir L edge strongly favors on-site excitations such as the single spin-orbit exciton. However, a close look at the RIXS data of Na_2IrO_3 reveals a small feature at about twice the energy of the spin-orbit exciton [25].

Triple spin-orbit exciton. A triple spin-orbit exciton excitation is possible on three neighboring sites i, j, k of the honeycomb lattice. It results from nearest-neighbor hopping t from i to j and from j to k and next-nearest-neighbor hopping t' from k to i (see Fig. 1). Following the logic of Lorenzana-Sawatzky-type phonon-assisted absorption [49,50], the different hopping amplitudes, in combination with the absence of inversion symmetry for this group of three sites, result in a finite dipole moment, i.e., the excitation is directly infrared active.

A triple excitation is unusual as the spectral weight strongly decreases with increasing particle number. In the present case, this is partially compensated by the fact that a directly infrared-active process such as the triple excitation is much stronger than phonon-assisted processes such as the single and double excitations. Moreover, next-nearest-neighbor hopping is of considerable size in α-$RuCl_3$, which is partially

caused by the strong hopping between the large Cl ions. Band-structure calculations find $t'/t \approx 0.38$ [45].

In conclusion, we solved a long-standing puzzle concerning the low-energy electronic structure of α-$RuCl_3$. The prominent features below the Mott gap can be identified as single, double, and triple spin-orbit excitons. In α-$RuCl_3$, the spin-orbit exciton is far below the gap, which allows Raman scattering and infrared absorption to take over the important role that RIXS plays in iridates. We determine $\lambda = 0.16$ eV, a central parameter for the theoretical modeling of α-$RuCl_3$, and $\Delta = 42(4)$ meV, corroborating the $j = 1/2$ scenario. The observation of a double spin-orbit exciton highlights the prominent role of Kitaev coupling and calls for studies of the interactions between excited $j = 3/2$ states in Kitaev materials.

We acknowledge funding from the Deutsche Forschungsgemeinschaft (DFG, German Research Foundation) – Project No. 277146847 – CRC 1238 (Projects A02, B02, B03, and C02).

[1] A. Kitaev, Anyons in an exactly solved model and beyond, Ann. Phys. **321**, 2 (2006).

[2] K. O'Brien, M. Hermanns, and S. Trebst, Classification of gapless Z_2 spin liquids in three-dimensional Kitaev models, Phys. Rev. B **93**, 085101 (2016).

[3] G. Jackeli and G. Khaliullin, Mott Insulators in the Strong Spin-Orbit Coupling Limit: From Heisenberg to a Quantum Compass and Kitaev Models, Phys. Rev. Lett. **102**, 017205 (2009).

[4] K. W. Plumb, J. P. Clancy, L. J. Sandilands, V. Vijay Shankar, Y. F. Hu, K. S. Burch, H.-Y. Kee, and Y.-J. Kim, α-$RuCl_3$: A spin-orbit assisted Mott insulator on a honeycomb lattice, Phys. Rev. B **90**, 041112(R) (2014).

[5] W. Witczak-Krempa, G. Chen, Y. B. Kim, and L. Balents, Correlated quantum phenomena in the strong spin-orbit regime, Annu. Rev. Condens. Matter Phys. **5**, 57 (2014).

[6] J. G. Rau, E. K.-H. Lee, and H.-Y. Kee, Spin-orbit physics giving rise to novel phases in correlated systems: Iridates and related materials, Annu. Rev. Condens. Matter Phys. **7**, 195 (2016).

[7] S. M. Winter, A. A. Tsirlin, M. Daghofer, J. van den Brink, Y. Singh, P. Gegenwart, and R. Valentí, Models and materials for generalized Kitaev magnetism, J. Phys.: Condens. Matter **29**, 493002 (2017).

[8] S. Trebst, Kitaev Materials, arXiv:1701.07056.

[9] M. Hermanns, I. Kimchi, and J. Knolle, Physics of the Kitaev model: fractionalization, dynamical correlations, and material connections, Annu. Rev. Condens. Matter Phys. **9**, 17 (2018).

[10] H. Takagi, T. Takayama, G. Jackeli, G. Khaliullin and S. E. Nagler, Concept and realization of Kitaev quantum spin liquids, Nat. Rev. Phys. **1**, 264 (2019).

[11] M. Majumder, M. Schmidt, H. Rosner, A. A. Tsirlin, H. Yasuoka, and M. Baenitz, Anisotropic $Ru^{3+}4d^5$ magnetism in the α-$RuCl_3$ honeycomb system: Susceptibility, specific heat, and zero-field NMR, Phys. Rev. B **91**, 180401(R) (2015).

[12] R. D. Johnson, S. C. Williams, A. A. Haghighirad, J. Singleton, V. Zapf, P. Manuel, I. I. Mazin, Y. Li, H. O. Jeschke, R. Valentí, and R. Coldea, Monoclinic crystal structure of α-$RuCl_3$ and the zigzag antiferromagnetic ground state, Phys. Rev. B **92**, 235119 (2015).

[13] S. M. Winter, K. Riedl, P. A. Maksimov, A. L. Chernyshev, A. Honecker, and R. Valentí, Breakdown of magnons in a strongly spin-orbital coupled magnet, Nat. Commun. **8**, 1152 (2017).

[14] A. Banerjee, C. A. Bridges, J.-Q. Yan, A. A. Aczel, L. Li, M. B. Stone, G. E. Granroth, M. D. Lumsden, Y. Yiu, J. Knolle, S. Bhattacharjee, D. L. Kovrizhin, R. Moessner, D. A. Tennant, D. G. Mandrus, and S. E. Nagler, Proximate Kitaev quantum spin liquid behaviour in a honeycomb magnet, Nat. Mater. **15**, 733 (2016).

[15] A. Banerjee, J. Yan, J. Knolle, C. A. Bridges, M. B. Stone, M. D. Lumsden, D. G. Mandrus, D. A. Tennant, R. Moessner, and S. E. Nagler, Neutron scattering in the proximate quantum spin liquid α-$RuCl_3$, Science **356**, 1055 (2017).

[16] L. J. Sandilands, Y. Tian, K. W. Plumb, Y.-J. Kim, and K. S. Burch, Scattering Continuum and Possible Fractionalized Excitations in α-$RuCl_3$, Phys. Rev. Lett. **114**, 147201 (2015).

[17] A. Glamazda, P. Lemmens, S.-H. Do, Y. S. Kwon, and K.-Y. Choi, Relation between Kitaev magnetism and structure in α-$RuCl_3$, Phys. Rev. B **95**, 174429 (2017).

[18] Y. Wang, G. B. Osterhoudt, Y. Tian, P. Lampen-Kelley, A. Banerjee, T. Goldstein, J. Yan, J. Knolle, H. Ji, R. J. Cava, J. Nasu, Y. Motome, S. E. Nagler, D. Mandrus, and K. S. Burch, The range of non-Kitaev terms and fractional particles α-$RuCl_3$, npj Quantum Mater. **5**, 14 (2020).

[19] A. Little, L. Wu, P. Lampen-Kelley, A. Banerjee, S. Patankar, D. Rees, C. A. Bridges, J.-Q. Yan, D. Mandrus, S. E. Nagler, and J. Orenstein, Antiferromagnetic Resonance and Terahertz Continuum in α-$RuCl_3$, Phys. Rev. Lett. **119**, 227201 (2017).

[20] Z. Wang, S. Reschke, D. Hüvonen, S.-H. Do, K.-Y. Choi, M. Gensch, U. Nagel, T. Rõõm, and A. Loidl, Magnetic Excitations and Continuum of a Possibly Field-Induced Quantum Spin Liquid in α-$RuCl_3$, Phys. Rev. Lett. **119**, 227202 (2017).

[21] J. Nasu, J. Knolle, D. L. Kovrizhin, Y. Motome, and R. Moessner, Fermionic response from fractionalization in an insulating two-dimensional magnet, Nat. Phys. **12**, 912 (2016).

[22] Y. Kasahara, T. Ohnishi, Y. Mizukami, O. Tanaka, S. Ma, K. Sugii, N. Kurita, H. Tanaka, J. Nasu, Y. Motome, T. Shibauchi, and Y. Matsuda, Majorana quantization and half-integer thermal quantum Hall effect in a Kitaev spin liquid, Nature (London) **559**, 227 (2018).

[23] J. Kim, D. Casa, M. H. Upton, T. Gog, Y.-J. Kim, J. F. Mitchell, M. van Veenendaal, M. Daghofer, J. van den Brink, G. Khaliullin, and B. J. Kim, Magnetic Excitation Spectra of Sr_2IrO_4 Probed by Resonant Inelastic X-Ray Scattering: Establishing Links to Cuprate Superconductors, Phys. Rev. Lett. **108**, 177003 (2012).

[24] J. Kim, M. Daghofer, A. H. Said, T. Gog, J. van den Brink, G. Khaliullin, and B. J. Kim, Excitonic quasiparticles in a spin-orbit Mott insulator, Nat. Commun. **5**, 4453 (2014).

[25] H. Gretarsson, J. P. Clancy, X. Liu, J. P. Hill, E. Bozin, Y. Singh, S. Manni, P. Gegenwart, J. Kim, A. H. Said, D. Casa,

T. Gog, M. H. Upton, H.-S. Kim, J. Yu, V. M. Katukuri, L. Hozoi, J. van den Brink, and Y.-J. Kim, Crystal-Field Splitting and Correlation Effect on the Electronic Structure of A_2IrO_3, Phys. Rev. Lett. **110**, 076402 (2013).

[26] M. Rossi, M. Retegan, C. Giacobbe, R. Fumagalli, A. Efimenko, T. Kulka, K. Wohlfeld, A. I. Gubanov, and M. Moretti Sala, Possibility to realize spin-orbit-induced correlated physics in iridium fluorides, Phys. Rev. B **95**, 235161 (2017).

[27] A. Revelli, C. C. Loo, D. Kiese, P. Becker, T. Fröhlich, T. Lorenz, M. Moretti Sala, G. Monaco, F. L. Buessen, J. Attig, M. Hermanns, S. V. Streltsov, D. I. Khomskii, J. van den Brink, M. Braden, P. H. M. van Loosdrecht, S. Trebst, A. Paramekanti, and M. Grüninger, Spin-orbit entangled $j = 1/2$ moments in Ba_2CeIrO_6: A frustrated fcc quantum magnet, Phys. Rev. B **100**, 085139 (2019).

[28] H. Gretarsson, H. Suzuki, Hoon Kim, K. Ueda, M. Krautloher, B. J. Kim, H. Yava, G. Khaliullin, and B. Keimer, Observation of spin-orbit excitations and Hund's multiplets in Ca_2RuO_4, Phys. Rev. B **100**, 045123 (2019).

[29] B. W. Lebert, S. Kim, V. Bisogni, I. Jarrige, A. M. Barbour, and Y.-J. Kim, Resonant inelastic x-ray scattering study of α-$RuCl_3$: A progress report, J. Phys.: Condens. Matter **32**, 144001 (2020).

[30] L. J. Sandilands, Y. Tian, A. A. Reijnders, H.-S. Kim, K. W. Plumb, Y.-J. Kim, H.-Y. Kee, and K. S. Burch, Spin-orbit excitations and electronic structure of the putative Kitaev magnet α-$RuCl_3$, Phys. Rev. B **93**, 075144 (2016).

[31] L. Binotto, I. Pollini, and G. Spinol, Optical and transport properties of the magnetic semiconductor α-$RuCl_3$, Phys. Status Solidi B **44**, 245 (1971).

[32] G. Guizzetti, E. Reguzzoni, and I. Pollini, Fundamental optical properties of α-$RuCl_3$, Phys. Lett. A **70**, 34 (1979).

[33] S. Reschke, F. Mayr, Z. Wang, S.-H. Do, K.-Y. Choi, and A. Loidl, Electronic and phonon excitations in α-$RuCl_3$, Phys. Rev. B **96**, 165120 (2017).

[34] Y. Hasegawa, T. Aoyama, K. Sasaki, Y. Ikemoto, T. Moriwaki, T. Shirakura, R. Saito, Y. Imai, and K. Ohgushi, Two-phonon absorption spectra in the layered honeycomb compound α-$RuCl_3$, J. Phys. Soc. Jpn. **86**, 123709 (2017).

[35] S. Reschke, F. Mayr, S. Widmann, H.-A. Krug von Nidda, V. Tsurkan, M. V. Eremin, S.-H. Do, K.-Y. Choi, Z. Wang, and A. Loidl, Sub-gap optical response in the Kitaev spin-liquid candidate α-$RuCl_3$, J. Phys.: Condens. Matter **30**, 475604 (2018).

[36] I. Pollini, Photoemission study of the electronic structure of $CrCl_3$ and $RuCl_3$ compounds, Phys. Rev. B **50**, 2095 (1994).

[37] H.-S. Kim, V. Shankar, A. Catuneanu, and H.-Y. Kee, Kitaev magnetism in honeycomb $RuCl_3$ with intermediate spin-orbit coupling, Phys. Rev. B **91**, 241110(R) (2015).

[38] L. J. Sandilands, C. H. Sohn, H. J. Park, S. Y. Kim, K. W. Kim, J. A. Sears, Y.-J. Kim, and T. W. Noh, Optical probe of Heisenberg-Kitaev magnetism in α-$RuCl_3$, Phys. Rev. B **94**, 195156 (2016).

[39] A. Koitzsch, C. Habenicht, E. Müller, M. Knupfer, B. Büchner, H. C. Kandpal, J. van den Brink, D. Nowak, A. Isaeva, and Th. Doert, J_{eff} Description of the Honeycomb Mott Insulator α-$RuCl_3$, Phys. Rev. Lett. **117**, 126403 (2016).

[40] A. Koitzsch, E. Müller, M. Knupfer, B. Büchner, D. Nowak, A. Isaeva, T. Doert, M. Grüninger, S. Nishimoto, and J. van den Brink, Low temperature enhancement of ferromagnetic Kitaev correlations in α-$RuCl_3$, Phys. Rev. Materials **4**, 094408 (2020).

[41] T. Biesner, S. Biswas, W. Li, Y. Saito, A. Pustogow, M. Altmeyer, A. U. B. Wolter, B. Büchner, M. Roslova, T. Doert, S. M. Winter, R. Valentí, and M. Dressel, Detuning the honeycomb of α-$RuCl_3$: Pressure-dependent optical studies reveal broken symmetry, Phys. Rev. B **97**, 220401(R) (2018).

[42] S. Agrestini, C.-Y. Kuo, K.-T. Ko, Z. Hu, D. Kasinathan, H. B. Vasili, J. Herrero-Martin, S. M. Valvidares, E. Pellegrin, L.-Y. Jang, A. Henschel, M. Schmidt, A. Tanaka, and L. H. Tjeng, Electronically highly cubic conditions for Ru in α-$RuCl_3$, Phys. Rev. B **96**, 161107(R) (2017).

[43] R. Yadav, N. A. Bogdanov, V. M. Katukuri, S. Nishimoto, J. van den Brink, and L. Hozoi, Kitaev exchange and field-induced quantum spin-liquid states in honeycomb α-$RuCl_3$, Sci. Rep. **6**, 37925 (2016).

[44] W. Wang, Z.-Y. Dong, S.-L. Yu, and J.-X. Li, Theoretical investigation of magnetic dynamics in α-$RuCl_3$, Phys. Rev. B **96**, 115103 (2017).

[45] S. M. Winter, Y. Li, H. O. Jeschke, and R. Valentí, Challenges in design of Kitaev materials: Magnetic interactions from competing energy scales, Phys. Rev. B **93**, 214431 (2016).

[46] Winter *et al.* [45] report the crystal-field parameters $\Delta_1 = -19.8$ meV, $\Delta_2 = -17.5$ meV, and $\Delta_3 = -12.5$ meV with energies E_i of the pure crystal-field Hamiltonian of $-\Delta_1$ and $\frac{1}{2}(\Delta_1 + \Delta_3 \pm \sqrt{(\Delta_1 - \Delta_3)^2 + 8\Delta_2^2})$. This yields $E_1 = -41.2$ meV, $E_2 = 8.9$ meV, $E_3 = 19.8$ meV, and $\Delta_{\text{CF}} \approx (E_2 + E_3)/2 - E_1 \approx 55$ meV. With our result for λ, this is equivalent to $\Delta \approx \frac{2}{3}\Delta_{\text{CF}} \approx 37$ meV.

[47] J. Chaloupka and G. Khaliullin, Hidden symmetries of the extended Kitaev-Heisenberg model: Implications for the honeycomb-lattice iridates A_2IrO_3, Phys. Rev. B **92**, 024413 (2015).

[48] B. H. Kim, T. Shirakawa, and S. Yunoki, From a Quasimolecular Band Insulator to a Relativistic Mott Insulator in t_{2g}^5 Systems with a Honeycomb Lattice Structure, Phys. Rev. Lett. **117**, 187201 (2016).

[49] J. Lorenzana and G. A. Sawatzky, Phonon Assisted Multimagnon Optical Absorption and Long Lived Two-Magnon States in Undoped Lamellar Copper Oxides, Phys. Rev. Lett. **74**, 1867 (1995).

[50] J. Lorenzana and G. A. Sawatzky, Theory of phonon-assisted multimagnon optical absorption and bimagnon states in quantum antiferromagnets, Phys. Rev. B **52**, 9576 (1995).

[51] J.-A. Yang, Y.-P. Huang, M. Hermele, T. Qi, G. Cao, and D. Reznik, High-energy electronic excitations in Sr_2IrO_4 observed by Raman scattering, Phys. Rev. B **91**, 195140 (2015).

[52] B. Henderson and G. F. Imbusch, *Optical Spectroscopy of Inorganic Solids* (Oxford University Press, Oxford, 1989).

[53] R. Rückamp, E. Benckiser, M. W. Haverkort, H. Roth, T. Lorenz, A. Freimuth, L. Jongen, A. Möller, G. Meyer, P. Reutler, B. Büchner, A. Revcolevschi, S.-W. Cheong, C. Sekar, G. Krabbes, and M. Grüninger, Optical study of orbital excitations in transition-metal oxides, New J. Phys. **7**, 144 (2005).

[54] R. K. Yoo and T. A. Keiderling, Intraconfigurational absorption spectroscopy of $IrCl_6^{2-}$ and IrB_6^{2-} in A_2MX_6-type host crystals, Chem. Phys. **108**, 317 (1986).

[55] A previous SW analysis of a different data set was reported in the Ph.D. thesis of one of the authors, N. Borgwardt [64]. This analysis finds phonon energies of 25 meV for peak A, 40 meV for peak B, and that peak C is not phonon assisted, in good agreement with our claims.

[56] E. M. Plotnikova, M. Daghofer, J. van den Brink, and K. Wohlfeld, Jahn-Teller Effect in Systems with Strong On-Site Spin-Orbit Coupling, Phys. Rev. Lett. **116**, 106401 (2016).

[57] Y. Sizyuk, C. Price, P. Wölfle, and N. B. Perkins, Importance of anisotropic exchange interactions in honeycomb iridates: Minimal model for zigzag antiferromagnetic order in Na_2IrO_3, Phys. Rev. B **90**, 155126 (2014).

[58] S. Sinn, C. H. Kim, B. H. Kim, K. D. Lee, C. J. Won, J. S. Oh, M. Han, Y. J. Chang, N. Hur, H. Sato, B.-G. Park, C. Kim, H.-D. Kim, and T. W. Noh, Electronic structure of the Kitaev material α-$RuCl_3$ probed by photoemission and inverse photoemission spectroscopies, Sci. Rep. **6**, 39544 (2016).

[59] M. Grüninger, M. Windt, E. Benckiser, T. S. Nunner, K. P. Schmidt, G. S. Uhrig, and T. Kopp, Optical spectroscopy of low-dimensional quantum spin systems, Adv. Solid State Phys. **43**, 95 (2003).

[60] In leading order one finds $q_{\rm eff} \propto ea\frac{J}{\Delta_{is}^2}\frac{\partial \Delta E_M}{\partial u}$, where e denotes the electric charge, a the metal-metal distance, Δ_{is} the effective intersite excitation energy, and ΔE_M the phonon-induced difference in metal on-site energies. In the cuprates, exchange is an order of magnitude larger than in α-$RuCl_3$, and Δ_{is} is about a factor of 2 larger. We thus find that $q_{\rm eff}$ is of the same order of magnitude.

[61] E. Benckiser, R. Rückamp, T. Möller, T. Taetz, A. Möller, A. A. Nugroho, T. T. M. Palstra, G. S. Uhrig, and M. Grüninger, Collective orbital excitations in orbitally ordered YVO_3 and $HoVO_3$, New J. Phys. **10**, 053027 (2008).

[62] See Supplemental Material at http://link.aps.org/supplemental/10.1103/PhysRevResearch.2.042007 for a theoretical analysis of interaction effects on the weight of the double spin-orbit exciton and for an exact diagonalization study of a two-site cluster.

[63] M. Windt, M. Grüninger, T. Nunner, C. Knetter, K. P. Schmidt, G. S. Uhrig, T. Kopp, A. Freimuth, U. Ammerahl, B. Büchner, and A. Revcolevschi, Observation of Two-Magnon Bound States in the Two-Leg Ladders of $(Ca, La)_{14}Cu_{24}O_{41}$, Phys. Rev. Lett. **87**, 127002 (2001).

[64] N. Borgwardt, Optics on materials with strong spin-orbit coupling: topological insulators $Bi_{2-x}Sb_xTe_{3-y}Se_y$ and the $j = 1/2$ compounds Na_2IrO_3 and α-$RuCl_3$, Ph.D. thesis, University of Cologne, 2019.